JOURNAL OF GEOPHYSICAL RESEARCH, VOL. 111, C08018, doi:10.1029/2005JC002954, 2006

Click Here for Full Article

Physical and biological contributions to the western tropical North Atlantic Ocean carbon sink formed by the Amazon River plume

S. R. Cooley[1] and P. L. Yager[1]

Received 11 March 2005; revised 27 March 2006; accepted 8 May 2006; published 19 August 2006.

[1] Dissolved inorganic carbon (DIC) and total alkalinity (TA) were measured in the upper 1000 m of the western tropical North Atlantic Ocean (WTNA; study area 3–15°N, 40–59°W) in January–February and July–August 2001. Concentrations of DIC and TA in surface samples (0–10 m) influenced by the Amazon River plume were up to 400 μmol C kg^{-1} (~20%) lower than oceanic surface samples. In this region, physical dilution by river water dominates DIC and TA inventories, driving CO_2 partial pressure (pCO_2) well below atmospheric levels. Nevertheless, DIC concentrations at most plume-influenced stations were 10–90 μmol C kg^{-1} below levels expected from conservative mixing of seawater with low-salinity, low-CO_2 Amazon River water. In this otherwise oligotrophic region, the diazotrophs *Trichodesmium spp*. and *Richelia intracellularis* were often abundant, supporting a link between increased carbon drawdown and nitrogen fixation in the outer plume. Net community production in the plume must surpass the fluxes of inorganic carbon from below and air-sea CO_2 replacement to leave biologically mediated DIC deficits, which is possible under observed conditions. Biological activity lowers plume pCO_2 30–120 μatm below the conservative mixing line, and contributes to a CO_2 deficit in the northern WTNA that outlasts the plume's physical structure.

Citation: Cooley, S. R., and P. L. Yager (2006), Physical and biological contributions to the western tropical North Atlantic Ocean carbon sink formed by the Amazon River plume, *J. Geophys. Res.*, *111*, C08018, doi:10.1029/2005JC002954.

1. Introduction

[2] The Amazon River discharge creates a 5–10 m deep plume of low-salinity, low-inorganic carbon water atop the western tropical North Atlantic (WTNA [*Nittrouer and Demaster*, 1986; *Lentz and Limeburner*, 1995; *Ternon et al.*, 2000]), forming a sink for atmospheric carbon covering approximately two million square kilometers [*Körtzinger*, 2003]. Tropical Atlantic seawater normally releases CO_2 to the atmosphere (0.15 Pg C yr^{-1} [*Takahashi et al.*, 2002]) because solubility-driven degassing exceeds biological production in lower latitudes [*Goyet et al.*, 1998; *Lee et al.*, 1997; *Takahashi et al.*, 1997, 2002; *Sarmiento et al.*, 1995]. In contrast, the Amazon carbon sink removes an estimated 0.014 ± 0.005 Pg C yr^{-1} (0.001 Pmol C yr^{-1} [*Körtzinger*, 2003]) from the atmosphere. Plume CO_2 uptake averages 1.35 mmol C m^{-2} d^{-1}, compared to the tropical Atlantic average loss of 1.84 mmol C m^{-2} d^{-1} [*Körtzinger*, 2003]. Since the Amazon River's discharge and biogeochemistry are apt to vary with changing climate, understanding the present and future WTNA carbon sink requires quantifying mechanistic controls on regional carbon fluxes.

[3] Rivers and ocean margins supply the ocean with organic carbon [*Bauer et al.*, 1995], fueling heterotrophy near the coast. Coastal regions become autotrophic when inorganic nutrients are abundant from upwelling or runoff [*Mackenzie et al.*, 1998]. The Amazon River delivers high concentrations of both nutrients and organic matter to the WTNA [*Smith and DeMaster*, 1996; *Demaster et al.*, 1996; *Ternon et al.*, 2000; *Körtzinger*, 2003]. Simultaneously, the river fosters primary production on the continental shelf [*Demaster and Pope*, 1996] and promotes CO_2 release via photooxidation or respiration of terrestrial organic matter in the WTNA [*Aller et al.*, 1996; *Demaster and Aller*, 2001; *Smith and DeMaster*, 1996; *Benner et al.*, 1995; *Del Vecchio and Subramaniam*, 2004]. The balance between oceanic heterotrophy and autotrophy, influenced by community structure [*Serret et al.*, 2001], determines the magnitude and direction of the air-sea CO_2 flux [*del Giorgio et al.*, 1997; *Duarte and Agustí*, 1998; *Williams*, 1998; *Geider*, 1997; *Williams and Bowers*, 1999; *Duarte et al.*, 2001]. Frequent diazotroph blooms in the WTNA may foster CO_2 drawdown directly or by fertilizing other autotrophs with biologically available nitrogen [*Capone et al.*, 1997; *Carpenter et al.*, 1999]. The resulting plume photosynthesis:respiration balance will then intensify or weaken the CO_2 sink created by the discharge of undersaturated river water. Quantifying total dissolved inorganic carbon (DIC) in seawater constrains biological variables, such as the magnitudes of net community production and organic carbon export [*Bender et al.*, 1987; *Yager et al.*, 1995; *Sweeney et al.*, 2000], but accounting for biological processes in the Amazon plume carbon sink depends first on distinguishing them from physical mixing effects in the WTNA.

[1]School of Marine Programs, University of Georgia, Athens, Georgia, USA.

Copyright 2006 by the American Geophysical Union.
0148-0227/06/2005JC002954$09.00

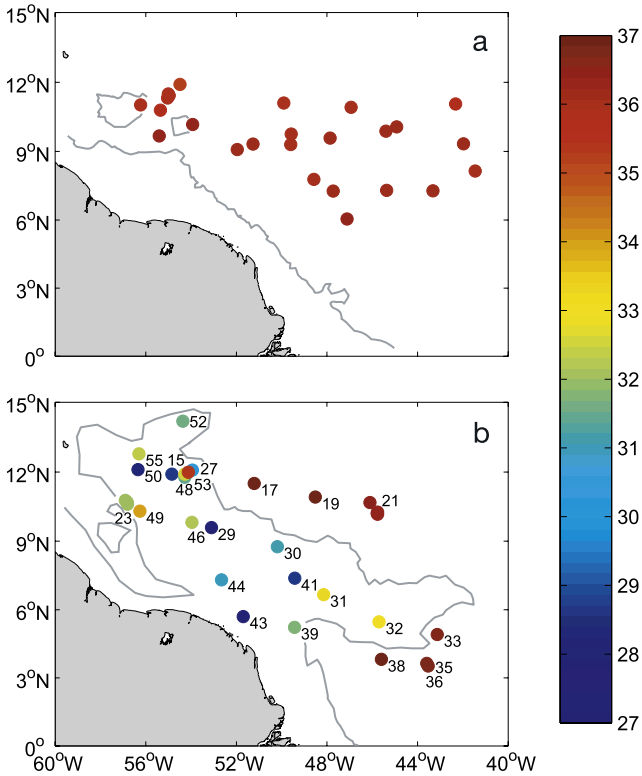

Figure 1. Map of (a) winter 2001 and (b) summer 2001 sea surface salinities (summer station numbers noted) in the western tropical North Atlantic Ocean. The gray line approximately follows the salinity 35 contour of the plume edge, generated using a correlation between K_{490} and salinity [*Del Vecchio and Subramaniam*, 2004] and satellite-derived monthly climatology of K_{490} (February and August), provided by A. Subramaniam.

[4] We collected vertical profiles of discrete DIC and TA samples in winter and summer 2001 with the NSF Biocomplexity MANTRA/PIRANA Project, which examined influences on WTNA diazotrophs. Our study took place between previously studied on-shelf and offshore plume-influenced areas [*Ternon et al.*, 2000; *Körtzinger*, 2003]. Winter samples from this region were not influenced by the plume, whereas summer samples included both plume- and non-plume-influenced regions. In this paper, we test the null hypothesis that physical processes solely influence WTNA inorganic carbon distributions. If physical mixing is insufficient to explain observed variation, we hypothesize that the residual is due to biological processes. We present measured DIC and TA (1–500 m) with calculated surface CO_2 partial pressure (pCO_2). We then use a mechanistic approach to quantify significant variations in DIC not explained by physical processes, and we compare our findings to previous work in the WTNA.

2. Methods

2.1. Sampling

[5] The winter data set was collected during daily stations aboard the R/V *Seward Johnson I* throughout the first Atlantic MANTRA/PIRANA cruise (MP1; January 19–February 22, 2001), within 5–14°N, 40–59°W (Figure 1a). The summer data set was collected during the second Atlantic MANTRA/PIRANA cruise (MP3; July 9–August 19, 2001) aboard the R/V *Knorr*, within 3–15°N, 42–57°W (Figure 1b).

[6] During both cruises, water samples were collected from discrete depths using Niskin bottles between 1 and 1000 m, with occasional deep (up to 4000 m) casts to compare with historical data sets. DIC and TA samples were collected according to established protocols [*DOE*, 1997]. Winter samples were analyzed aboard ship within 1 week of sampling for DIC and TA. Summer samples were kept cool aboard ship until they were returned to Georgia, where they were stored in the dark at 4°C until processing. Seawater collected and stored following this protocol was stable for DIC and TA analysis for at least 4 years (P. L. Yager, unpublished data). Summer samples were analyzed within 2–3 months of collection.

2.2. Sample Analysis

2.2.1. DIC

[7] Dissolved inorganic carbon measurements were performed on a SOMMA system (Single Operator Multiparameter Metabolic Analyzer [*Johnson et al.*, 1993]) connected to a CO_2 coulometer (UIC, Inc. Model 5011). Samples were analyzed following standard protocols [*Johnson et al.*, 1993; *DOE*, 1997; *Bates et al.*, 1996]. Sample conductivity was measured with a Sea-Bird conductivity cell (SBE-4) plumbed into the SOMMA gas-driven delivery system. Salinity (practical salinity scale, unitless) was calculated based on cell calibration to IAPSO salinity standards.

[8] Primary system calibration was based on analysis of pure (99.995%) CO_2 gas and Certified Reference Materials (CRMs; supplied by A. G. Dickson, Scripps Institute of Oceanography). DIC measurements were corrected to daily standards. Instrument precision for the winter data set, based on analysis of replicate standards [*DOE*, 1997], was ±0.559 μmol C kg SW^{-1}, and precision based on replicate samples was ±0.832 μmol C kg SW^{-1}. Precisions for the summer data set were ±0.401 μmol C kg SW^{-1} and ±0.601 μmol C kg SW^{-1}, respectively.

2.2.2. TA

[9] Total alkalinity was measured using a programmable open-cell potentiometric titration system [*Dickson et al.*, 2003; *Bates et al.*, 1996]. Winter samples analyzed aboard ship were dispensed with a 100 mL volumetric pipette; sample temperature was measured while filling, and sample mass was calculated [*Millero and Poisson*, 1981]. Summer samples analyzed on shore were weighed using an electronic balance accurate to within 0.06 g (0.05% of typical sample mass) with a precision of ±0.2 mg. Samples were titrated with small additions of 0.1 N HCl in 0.7 M NaCl and total alkalinity was determined with a modified Gran calculation [*Dickson et al.*, 2003; *Goyet et al.*, 1998; *Bates et al.*, 1996; *DOE*, 1997; *Millero et al.*, 1993].

[10] CRMs were used as primary alkalinity standards to back-calculate titration acid concentration. This forced the absolute accuracy of samples to CRM standards. Instrument precision for the winter data set based on replicate standards [*DOE*, 1997] was ±1.74 μequivalents kg SW^{-1}, while precision based on duplicate samples was ±2.97 μeq kg

SW^{-1}. For the summer data set, precisions were ±2.16 μeq kg SW^{-1}, and ±2.45 μeq kg SW^{-1}, respectively.

2.3. Data Analysis

2.3.1. pCO_2 Calculations

[11] Measurements of underway seawater CO_2 partial pressure were unavailable for these cruises, so partial pressure (pCO_2) at in situ temperature (pCO_2(SST)) or at 28°C (pCO_2(28)) was calculated from discrete, near-surface DIC and TA data using the computer program CO2SYS [*Lewis and Wallace*, 1998], which uses *Weiss* [1974] solubility. Calculating pCO_2 at 28 °C permitted comparing the inorganic carbon inventory between seasons, isolating changes from seasonal temperature effects. The operator-chosen constants used in CO2SYS calculations were: carbonate dissociation constants of *Mehrbach et al.* [1973], refit by *Dickson and Millero* [1987] (valid for salinities 20–40), and the KSO_4 dissociation constants from *Dickson* [1990]. Recalculation of pCO_2 at different temperatures and in situ salinity using CO2SYS was within 3% of the empirically based *Takahashi et al.* [1993] method (data not shown).

2.3.2. Plume Definition

[12] The Amazon plume near the north Brazilian shelf is a 5–10 m thick layer of low-salinity water separated from underlying oceanic water by a sharp, 5 m halocline [*Lentz and Limeburner*, 1995, and references therein], which creates a shallow surface mixed layer [*Pailler et al.*, 1999]. Because plume waters cannot be identified by geographic characteristics, plume-influenced stations in our summer 2001 data set were identified by their low surface salinities (<35) and shallow haloclines (<10 m [*Lentz and Limeburner*, 1995; *Lentz*, 1995; *Geyer*, 1991]). Because of the extremely shallow SML depths at plume stations, we usually collected samples at only one depth in the SML. Therefore, the "surface" and "SML" data groupings used herein are nearly equivalent. Nonplume surface waters in the WTNA, with no distinctive salinity or density features in the upper 80 m [*Lentz and Limeburner*, 1995] (also GEOSECS and WOCE data: details below), have salinities near 36 throughout the entire SML.

2.3.3. Statistics

[13] Mean values are reported with standard errors throughout this paper, unless otherwise noted; SML characteristics were compared using Welch's approximate t-test after F-tests detected significant differences between statistic variances [*Sokal and Rohlf*, 2000]. The critical value used in all statistical tests was $\alpha = 0.05$.

[14] Regressions against salinity were used to describe conservative mixing between plume and ocean water. Since both salinity and the inorganic carbon system are subject to natural variation and/or measurement error, Model II (reduced major axis) regression statistics were used throughout the analysis [*Sokal and Rohlf*, 2000]. Model II statistics are recalculated here for 0–15 m data from the ETAMBOT 1, 2 and SABORD cruises originally published by *Ternon et al.* [2000] (data obtained online: details below).

2.3.4. Supplementary Data

[15] Air-sea CO_2 gradients (ΔpCO_2; $pCO_2 - pCO_{2atm}$) were determined using calculated in situ surface pCO_2 (pCO_2) and the average atmospheric pCO_2 (pCO_{2atm}) for each cruise at Ragged Point, Barbados (NOAA CMDL; www.cmdl.noaa/gov/infodata/ftpdata.html/). "Winter" (Jan.–Feb.) and "summer" (Jul.–Aug.) pCO_{2atm} averaged 371.9 ± 0.6 μatm and 369.3 ± 1.0 μatm, respectively.

[16] Air-sea CO_2 fluxes were calculated using ΔpCO_2, solubility [*Weiss*, 1974], and piston velocity from the long term wind formulation of *Wanninkhof* [1992] at an average wind speed of 8 m s^{-1} (generalized from our data; see below).

[17] Average surface mixed layer (SML) depths were calculated from CTD profiles at each station using a density gradient criterion ($\Delta\rho/\Delta z = 0.01$, where ρ is density and z is depth) [*Brainerd and Gregg*, 1995]. Diazotrophic organism counts, nutrient measurements, and underway data were provided by MANTRA/PIRANA project collaborators (see Acknowledgments). Inorganic carbon data from the ETAMBOT 1, 2, and SABORD cruises [*Ternon et al.*, 2000] were obtained from the IFREMER FTP site (www.ifremer.fr/sismer). CO_2 fugacity (fCO_2, nearly equal to pCO_2 in seawater) from the *Meteor* 55 cruise [*Körtzinger*, 2003] were kindly provided by the author. NOAA NCEP NCAR reanalysis data [*Kalnay et al.*, 1996] were from the IRI-LDEO Climate Data Library (http://ingrid.ldeo.columbia.edu). GEOSECS and WOCE inorganic carbon data were obtained for comparison from IRI-LDEO (GEOSECS) or the Carbon Dioxide Information Analysis Center (http://cdiac.esd.ornl.gov/, WOCE).

2.3.5. PWP Mixed Layer Model for the Nonplume WTNA

[18] Daily mixed layer depths and average SML inorganic carbon inventory changes for the winter and summer non-plume-influenced WTNA were simulated using the Price-Weller-Pinkel mixed layer model for Matlab [*Price et al.*, 1986] (http://www.po.gso.uri.edu/rafos/research/pwp/). The summer non-plume-influenced WTNA was further divided into two groups: those stations south of the plume structure, with oversaturated pCO_2 (stations 33, 35, 36, 38) and those northeast of the plume structure, with undersaturated pCO_2 (stations 17, 19, 21). In each run, the model was initialized with a depth profile of mean temperature, salinity, DIC, and TA for that station group from CTD data and interpolated bottle data. Background vertical eddy diffusivity was set at 1×10^{-5} m^2 s^{-1} [*Ledwell et al.*, 1993]. Underway wind speed, relative humidity, short wave radiation, barometric pressure, and precipitation were unavailable for the winter cruise, so we forced the winter model with daily heat, fresh water, and momentum fluxes for the WTNA from the NCEP-NCAR reanalysis [*Kalnay et al.*, 1996]. Short wave radiation was unavailable for 2001 from NCEP-NCAR, so we used 2002 data. Heat fluxes driving the summer model runs were calculated following *Gill* [1982], using hourly mean underway wind speed, SST, air temperature, relative humidity, barometric pressure, precipitation, and short wave radiation. Wind stress was calculated following *Yelland and Taylor* [1996]. Mixed layer inorganic carbon inventory changes were estimated by treating DIC as a passive tracer that is affected by vertical flux and net evaporation/precipitation [*Sabine et al.*, 2004] but not by air-sea transfer or biology. Equations describing DIC mixing in the model were therefore based on corresponding equations for salt. The rates of change in mixed layer inventories were calculated between initial and final SML concentrations over the 31- or 32-day cruise interval modeled (winter

and summer, respectively). To estimate the impact of precipitation and evaporation on modeled SML DIC inventories, the three model runs were also performed with zero freshwater influence on DIC. The salinity budget was still influenced by freshwater to permit proper development of the modeled mixed layer. Modeled SML carbon inventory changes from the zero-freshwater runs represent only the vertical carbon flux, whereas DIC SML inventory changes calculated from the full runs represent the vertical carbon flux plus evaporation/precipitation-induced inventory changes.

2.3.6. Plume Physical Influences

[19] Plume mixed layer dynamics were not evaluated with the PWP vertical mixing model, because the plume's existence depends on horizontal mixing between low-salinity, low-carbon river water and surface WTNA water [*Lentz and Limeburner*, 1995]. In general, strong density stratification between the plume and underlying ocean water attenuates vertical mixing [*Pailler et al.*, 1999; *Sprintall and Tomczak*, 1992] and forces a shallow mixed layer, although background vertical diffusion may not weaken [*Ferry and Reverdin*, 2004]. During the plume's approximately 80-day transit from the Amazon mouth to the locations sampled [*Hellweger and Gordon*, 2002, and references therein], only gas exchange, the net effects of evaporation and precipitation, and horizontal mixing influence DIC. Plume water is therefore treated in this analysis as an isolated, vertically homogenous water mass atop the WTNA; its one-dimensional carbon budget is influenced by surface processes only, including gas exchange and export, with no acquisition of inorganic carbon via vertical mixing from below.

2.3.7. Mixing Model

[20] Building on the approaches of *Ternon et al.* [2000] and *Körtzinger* [2003], we used a simple conservative mixing model to calculate the proportions of Amazon plume water and seawater in a given plume sample. We assumed that the effects of precipitation and evaporation on the carbon and freshwater mass balances were small compared to the river [*Lentz*, 1995; *Lentz and Limeburner*, 1995] over a 10 m-deep plume (see section 3.5). Additional variations in DIC not attributable to mixing were then ascribed to biology. For each discrete SML sample collected, we solved the following system of equations for the proportions of river (r) and seawater (s) present:

$$S_r * r + S_s * s = S_{obs} \tag{1}$$

$$r + s = 1 \tag{2}$$

S_r, S_s and S_{obs} are salinities for the river endmember, the seawater endmember, and the observed sample, respectively.

[21] Assuming that alkalinity was conservative, the alkalinity of the river endmember was then calculated from each sample alkalinity (A_{obs}) and the oceanic alkalinity endmember (A_s), using r and s from above:

$$A_r = \frac{A_{obs} - A_s * s}{r} \tag{3}$$

Because the Amazon River mainstem DIC load is ~0% carbonate, 82% bicarbonate, and 18% dissolved CO_2 gas [*Richey et al.*, 1991; *Devol and Hedges*, 2001], the river DIC endmember (DIC_r) in our model was calculated to be:

$$DIC_r = \frac{A_r}{0.82} \tag{4}$$

[22] The expected inorganic carbon concentration for that sample (DIC_{ex}) was then calculated using r, s, and river (DIC_r) and seawater (DIC_s) endmembers:

$$DIC_{ex} = DIC_r * r + DIC_s * s \tag{5}$$

DIC_{ex}, A_{obs}, and in situ nutrient concentrations were then used to calculate the pCO_2 expected (pCO_{2ex}) from conservative mixing using CO2SYS. Nonconservative variations in DIC attributed to biology (ΔDIC_{BIO}) were the differences between expected and observed DIC values:

$$\Delta DIC_{BIO} = DIC_{ex} - DIC_{obs} \tag{6}$$

Positive ΔDIC_{BIO} values correspond to inorganic carbon deficits, implying that production exceeds respiration and the system is net autotrophic. Negative values indicate inorganic carbon surpluses, suggesting that respiration exceeds production, and the system is net heterotrophic. Errors in derived quantities were estimated using a Monte Carlo-type error analysis [see *Yager et al.*, 1995].

2.3.8. Model Endmembers

[23] Surface mixed layer DIC, TA, and salinity were averaged for the four southeastern summer nonplume stations to provide seawater endmember values and their standard deviations (A_s = 2369.4 ± 5.9, S_s = 36.0 ± 0.1, DIC_s = 2024.5 ± 6.8, n = 12). These stations (33, 35, 36, 38) were located in the North Brazil Current (NBC), the water mass that entrains the Amazon plume [*Bourles et al.*, 1999; *Johns et al.*, 1998]. River salinity (S_r) was assumed to equal 0 ± 0, as 0 psu salinity water has been documented outside of the river mouth [*Lentz*, 1995; *Lentz and Limeburner*, 1995; *Geyer et al.*, 1996; *Edmond et al.*, 1981]. The mixing line slope implied by this model was calculated using solved mean A_r, A_s, S_r, and S_s (or DIC_r, DIC_s, S_r, and S_s) and a Monte Carlo-type analysis [see *Yager et al.*, 1995] that kept track of error propagation.

3. Results

3.1. Observation

[24] DIC and TA concentrations in the Amazon plume-influenced upper WTNA were up to 400 μmol kg^{-1} lower than oceanic (nonplume) values (Table 1 and Figure 2a). Surface pCO_2 at in situ temperatures (pCO_2(SST)) was also about 50 μatm lower in the plume; the difference between plume and nonplume surface pCO_2 was enhanced when temperature differences were reconciled (Table 1; pCO_2(28°C)). This significant inorganic carbon reduction was always associated with low-density plume water atop the water column (σ_t = 17 − 23; Figure 2b). At nonplume stations, average surface mixed layer (SML) DIC, TA, salinity, SML depth, and pCO_2(28) were statistically indistinguishable between seasons (data not shown).

[25] Over the salinity range sampled, DIC and TA were linearly correlated to salinity (Table 2 and Figure 3a). The

Table 1. Mean Surface Mixed Layer (SML) Characteristics (±1SE) for Winter and Summer 2001[a]

	Nonplume	Plume
Stations	(n = 27)	(n = 18)
SML depth, m	78.0 ± 4.4	9.2 ± 1.5
SML samples	(n = 123)	(n = 25)
DIC, μmol C kg^{-1}	2017.2 ± 1.5	1786.2 ± 15.8
TA, μeq C kg^{-1}	2365.7 ± 1.2	2124.3 ± 19.7
Salinity	36.05 ± 0.02	31.91 ± 0.36
SST, °C	26.13 ± 0.08	28.68 ± 0.10
Surface samples	(n = 36)	(n = 21)
pCO_2(SST), μatm	359.5 ± 2.7	308.3 ± 8.3
pCO_2(28°C), μatm	383.9 ± 2.5	297.0 ± 8.4

[a]All plume means except pCO_2(SST) were significantly different ($p < 0.05$) from nonplume means (Welch's t-test).

relationship between plume TA and salinity was not significantly different from that of previously published data from the ETAMBOT/SABORD projects (fall 1995 and spring 1996 [*Ternon et al.*, 2000]) (Table 2). In addition, the residuals around the TA-salinity regression line are much smaller on the whole than the residuals around the DIC-salinity regression (Figure 3b).

[26] During the winter cruise, sea surface temperature (SST) and sea surface salinity (SSS) ranged between 20.9–26.6°C and 35.2–36.3, respectively (Figures 4a and 4b). Mixed layer depths ranged between 47 and 133 m (Figure 4c). Due to an equipment malfunction, underway wind speed was not archived for this cruise; wind speeds shown are from station logfiles, and range between 7–15 m s^{-1} (Figure 4d). During the summer cruise, SST ranged between 25.8–30.0°C and SSS ranged between 26.4–36.7 (Figures 4e and 4f). Lower SSS and higher SST were indicative of the Amazon plume (Figure 4 and Table 1). Summer mixed layer depths ranged between 2–103 m (Figure 4g). Summer wind speed ranged between 0 and 12 m s^{-1} (Figure 4h). Shallow MLDs in summer (<15 m) were always associated with SSS below 35.

3.2. Air-Sea CO_2 Gradients

[27] Air-sea CO_2 gradients in summer 2001 varied over a larger range (ΔpCO_2 = −135 to +30 μatm) than in winter (ΔpCO_2 = −48 to +10 μatm; Figure 5). Stations most undersaturated with respect to the atmosphere (negative ΔpCO_2; stations 23 and 27) were far from the river mouth, in the middle of the observed salinity range. The most oversaturated stations (positive ΔpCO_2; summer stations 33, 35, 36, 38) were outside plume-influenced waters. The only oversaturated station within plume water (station 43) was close to the river mouth and on the continental shelf. Station 43 was unusual in that, although salinity, DIC, and TA were characteristic of plume water, they were vertically homogenous throughout the 80 m water depth; no surface mixed layer was evident. Outside of the plume, the small significant difference observed between winter and summer mean pCO_2(SST) was partly attributable to seasonal changes in SST (Table 3). Winter pCO_2(SST) was undersaturated due to cool temperatures, but summer nonplume pCO_2(SST) was not uniformly oversaturated due to warm temperatures. Summer nonplume stations fell into two groups: stations whose pCO_2(SST) was greater than the atmospheric value (33, 35, 36, and 38, south of the plume; Figure 5b), and those whose pCO_2(SST) was less than atmospheric pCO_2 (15, 17, 19, and 21, north and east of the plume; Figure 5b; stations labeled on Figure 1b). The difference between the two summer groups' pCO_2(SST) was unrelated to temperature (Table 3), as the difference remained when temperature changes were reconciled. The overall mean nonplume pCO_2(SST) undersaturation (Table 1) resulted from grouping cooler, undersaturated winter stations with the two types of warmer summer stations.

3.3. Air-Sea Fluxes

[28] The mean flux at plume stations (ΔpCO_2 = −61.0 ± 8.3 μatm, salinity = 31.6 ± 0.4, SST = 28.8 ± 0.1°C, wind speed 8 m s^{-1}) was 9.7 ± 1.3 mmol C m^{-2} d^{-1} into the water. The air-sea fluxes at summer nonplume stations were quite different from the plume: south of the plume (ΔpCO_2 = 19.3 ± 4.4 μatm, salinity = 36.0 ± 0.06, SST = 27.4 ± 0.2°C, wind speed = 8 m s^{-1}), CO_2 was released to the atmosphere (mean flux = 3.0 ± 0.7 mmol C m^{-2} d^{-1}); north of the plume (ΔpCO_2 = −10.3 ± 0.7 μatm, salinity = 35.9 ± 0.09, SST = 27.6 ± 0.1°C, wind speed = 8 m s^{-1}), the average CO_2 flux was 1.6 ± 0.1 mmol C m^{-2} d^{-1} into the water, 6× lower than the rate for the plume. The average calculated air-sea CO_2 flux for winter nonplume stations

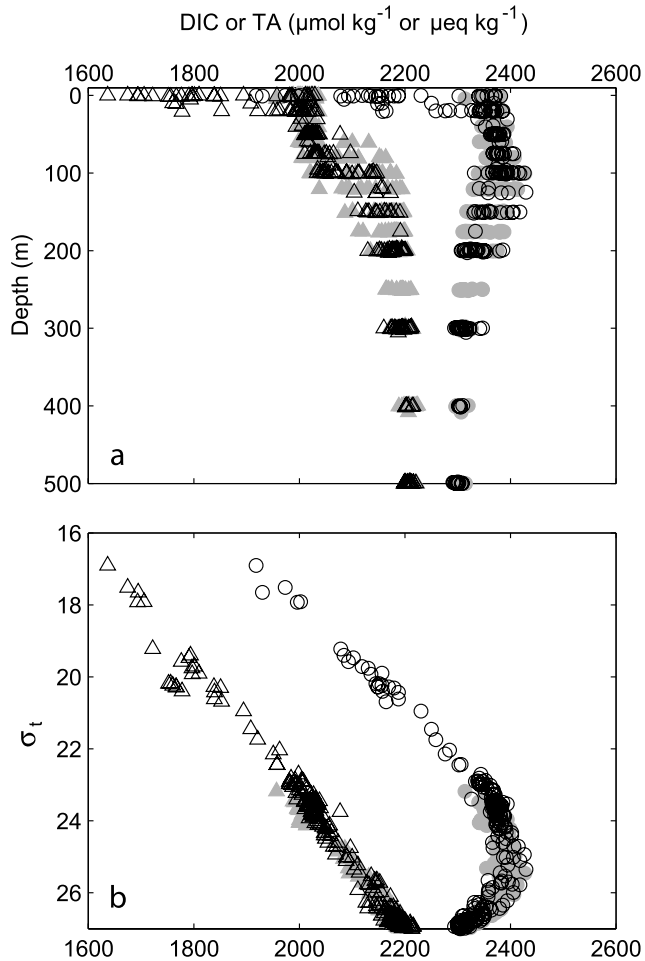

Figure 2. Winter (solid gray symbols) and summer 2001 (open black symbols) DIC (open triangles) and TA (open circles) in the WTNA plotted against (a) depth and (b) σ_t. σ_t = 27 is approximately 500 m.

Table 2. Model II Regression Statistics (±1 SE) for the Carbonate System Versus Salinity[a]

	DIC			TA		
	r[b]	slope	y-intercept	r	slope	y-intercept
Plume (n = 25)	0.912	44.1 ± 3.8	378.5 ± 120.4	0.983	55.0 ± 2.1	369.7 ± 68.1
ETAMBOT I, II, SABORD[c] (n = 158)	0.997	49.6 ± 0.3	223.6 ± 9.5	0.998	59.0 ± 0.3	268.4 ± 9.7
Mixing model (n = 25)[d]		47.6 ± 0.3	308.8 ± 11.6		58.8 ± 0.3	253.3 ± 9.5
Obidos river endmember[e]			600			600

[a]Slopes and intercepts for plume and ETAMBOT/SABORD groupings were significantly different from nonplume conditions.
[b]The parameter r is correlation coefficient; all correlations shown were significant.
[c]ETAMBOT 1, 2, and SABORD data (fall 1995, spring 1996) from *Ternon et al.* [2000] were pooled and analyzed using Model II regressions.
[d]Slope implied by mixing-model-generated y-intercepts and ocean endmembers (see Methods).
[e]Obidos river endmember used by *Ternon et al.* [2000], from *Richey et al.* [1990].

(ΔpCO_2 = −16.7 ± 2.8 μatm, salinity = 36.0 ± 0.05, SST = 25.9 ± 0.1°C, wind speed = 8 m s^{-1}) was 2.6 ± 0.4 mmol C m^{-2} d^{-1} into the water, only slightly greater than the northern summer nonplume stations. In the winter, observed wind speeds were generally greater than 8 m s^{-1} (7–15 m s^{-1}), so the in situ flux could be somewhat greater than estimated here (the effect would be amplified if we had applied the *Wanninkhof and McGillis* [1999] long-term formulation for the gas transfer velocity instead of *Wanninkhof* [1992], since the two formulations diverge above 8 m s^{-1}), whereas observed summer winds (1–12 m s^{-1}) could generate slightly lower fluxes than estimated here.

3.4. PWP Mixed Layer Model

[29] Winter SML depths from the PWP mixed layer model (Table 4) agreed favorably with SML depth observations. In winter, salinity increased in the SML at a rate of 0.003 d^{-1} (or ~0.01% d^{-1}). Carbon increased at a somewhat faster rate (0.36 μmol kg^{-1} d^{-1} or ~0.02% d^{-1}) because of the stronger vertical gradient in DIC. Integrating over the modeled mixed layer depth, the change in the integrated mixed layer salt inventory (storage) is 2.8 mg salt m^{-2} s^{-1} and the change in the mixed layer carbon inventory is 27 mmol C m^{-2} d^{-1}. Excluding the freshwater influence on winter SML DIC, the change in the carbon inventory was only 16 mmol C m^{-2} d^{-1}; net winter evaporation therefore concentrates SML DIC to cause the additional 11 mmol C m^{-2} d^{-1} increase (Table 4). The model predicted shallower mixed layers under late summer conditions than we observed at either group of summer nonplume stations. Calculated summer mixed layer depths were 15.0 ± 0.5 and 14.4 ± 0.4 (southern and northern groups, respectively),

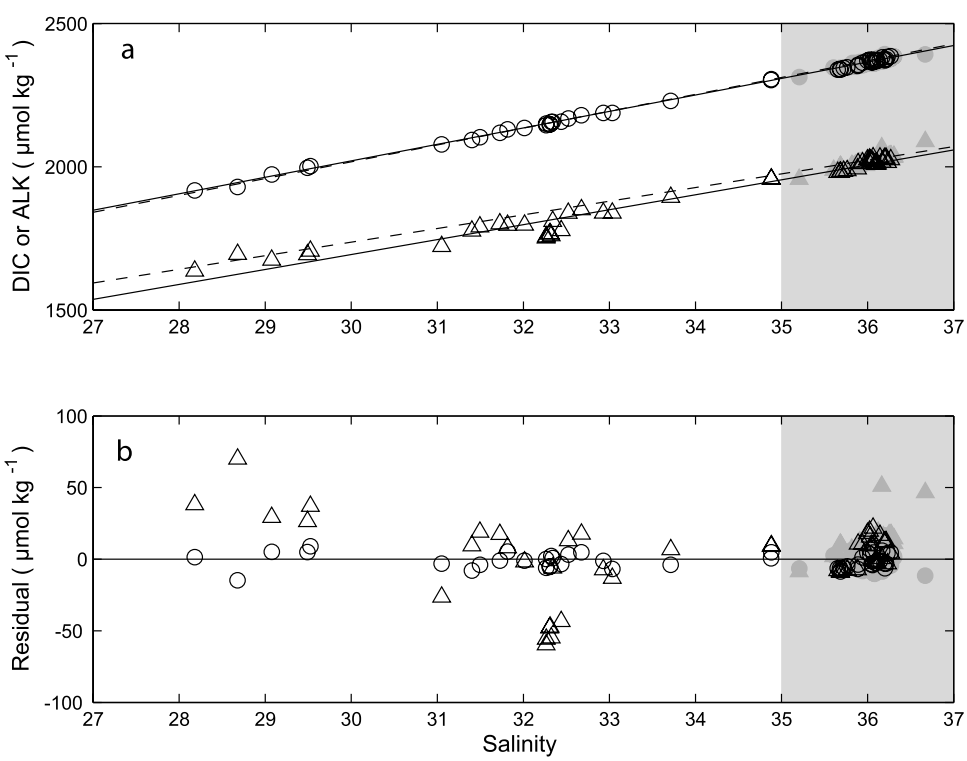

Figure 3. (a) DIC (open triangles) and TA (open circles) against salinity for summer 2001 (open symbols) and winter 2001 (solid gray symbols). The statistics for the plume-influenced solid regression lines shown are in Table 2. Dashed lines indicate mixing lines implied by the mixing model, whose slope and intercept are in Table 2. (b) Residual of summer and winter DIC and TA around the plume-influenced regressions. The shaded regions above salinity 35 indicate data outside the influence of the plume.

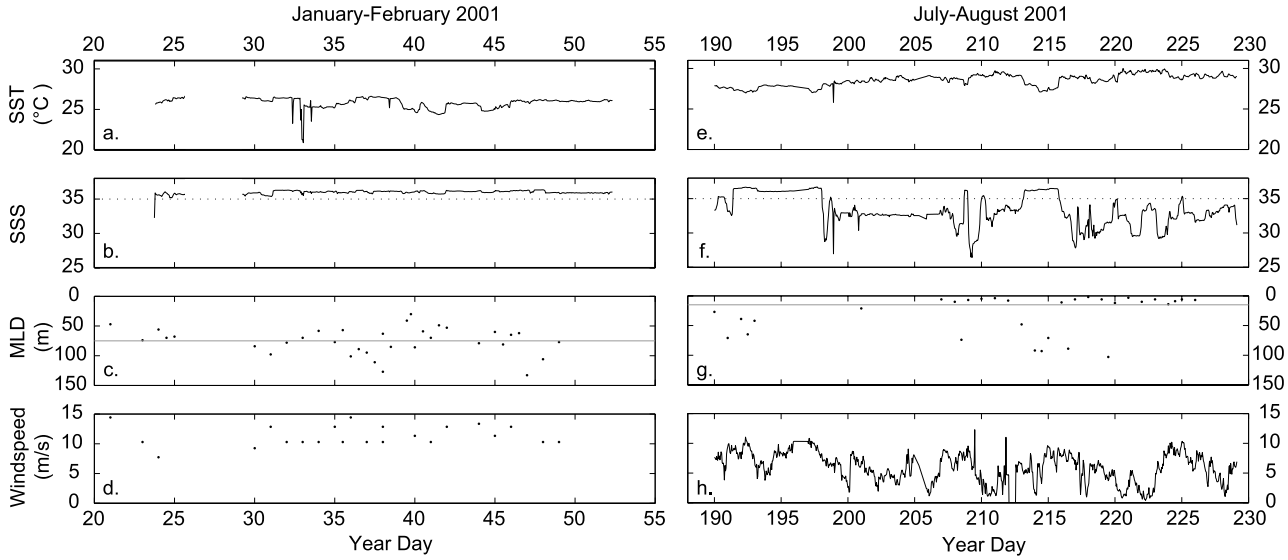

Figure 4. Winter (a–d) and summer (e–h) 2001 underway sea surface temperature (SST), sea surface salinity (SSS), observed mixed layer depth (MLD), and wind speed. The dotted lines in (b, f) indicate salinity 35, the threshold below which samples are considered "plume-influenced." The gray lines in (c, g) at MLDs 75 and 15 for winter and summer, respectively, indicate the modeled MLD for both seasons (see Results).

significantly shallower than the mean observed nonplume mixed layer depths of 54.3 ± 8.1 and 76.0 ± 10.6 m. Modeled summer mixed layer salinity decreased at a rate of 0.0005–0.0009 d^{-1}, and mixed-layer DIC decreased 0.01–0.03 μmol kg^{-1} d^{-1}. When integrated over the modeled mixed layer depth, the mixed layer salt inventory lost 0.1–0.2 mg m^{-2} s^{-1}, and the mixed layer DIC inventory lost 0.22–0.53 mmol m^{-2} d^{-1}. Excluding freshwater effects in summer, the SML DIC inventory increased 0.4–0.6 mmol C m^{-2} d^{-1} (southern and northern stations, respectively), so net precipitation decreased DIC inventories by 0.92–0.83 mmol C m^{-2} d^{-1}, respectively. A preliminary yearlong PWP model run forced with daily NCEP-NCAR data (results not shown) indicates that our observations were at the start of annual WTNA autumn mixed layer shoaling, when mixed layer depths oscillate rapidly.

3.5. Plume Physical Influences

[30] The average air-sea CO_2 flux into the plume (9.7 ± 1.3 mmol C m^{-2} d^{-1}) causes a DIC increase of 1.0 μmol C kg^{-1} d^{-1} in a 10 m plume. At the same time, late summer net precipitation (E-P = −1.4 ± 1.3 mm d^{-1}, calculated from the summer 2001 underway data) dilutes dissolved species and lowers DIC. Adding 1.4 mm d^{-1} or 1.4 L m^{-2} d^{-1} water to a 10 m mixed layer with DIC = 2100 μmol C kg^{-1} will lower DIC concentrations by 0.3 μmol C kg^{-1} d^{-1}. During the plume's approximately 80-day transit from the Amazon mouth to the locations sampled [*Hellweger and Gordon*, 2002, and references therein], mean air-sea transfer can therefore increase plume DIC by 80 μmol C kg^{-1} and net precipitation can decrease DIC by 24 μmol C kg^{-1}. In total (56 μmol C kg^{-1}), these physical processes contribute up to only 3.3% of the DIC acquired by a water parcel between the river (DIC_r = 308.8 μmol kg^{-1}, see below) and the offshore ocean (DIC_s = 2024.5 μmol kg^{-1}).

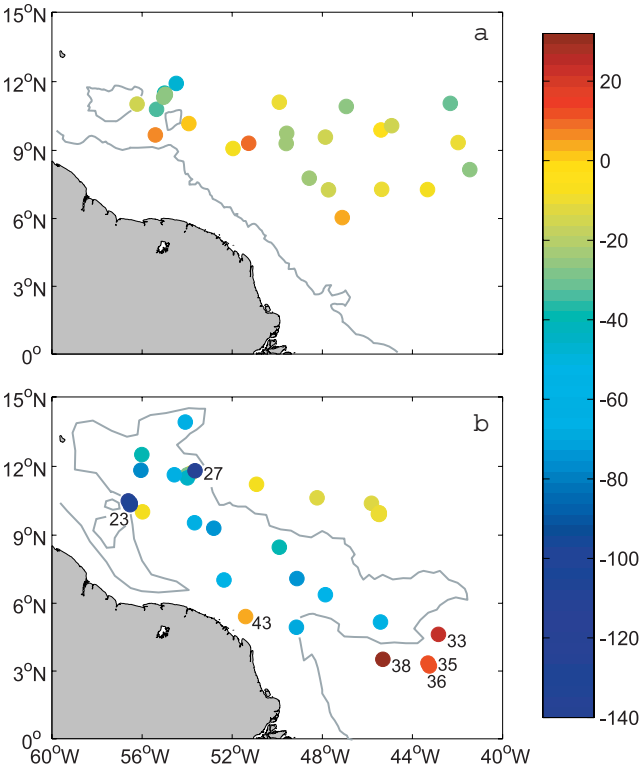

Figure 5. ΔpCO_2 (pCO_{2sea} (SST) − pCO_{2atm}; μatm), plotted on a map of the WTNA in (a) winter and (b) summer 2001. The gray line indicates the approximate location of the salinity 35 contour, also shown and described in Figure 1. Station numbers discussed in the text are noted. Stations with $+\Delta pCO_2$ (red-orange colors) are oversaturated with respect to the atmosphere; $-\Delta pCO_2$ (blue-green colors) represent undersaturated regions.

Table 3. Breakdown of pCO_2 Values (±1 SE) by Subgroup for Nonplume WTNA Samples

	All (n = 36)	Winter (n = 26)	Summer (n = 10)	Summer Southern[a] (n = 4)	Summer Northern[b] (n = 6)
SST	26.3 ± 0.2	**25.9 ± 1.0**[c]	**27.5 ± 0.0**	27.4 ± 0.2	27.6 ± 0.1
pCO_2(SST)	359.5 ± 2.7	**355.2 ± 2.8**	**370.8 ± 5.1**	**388.6 ± 4.4**	**359.0 ± 0.7**
pCO_2(28)	383.9 ± 2.5	386.3 ± 2.6	377.6 ± 5.6	**397.4 ± 3.0**	**364.4 ± 1.9**

[a]Includes stations 33, 35, 36, 38 (Figure 1).
[b]Includes stations 17, 19, 21 (Figure 1).
[c]Bold values indicate a significant difference (winter is compared with summer, summer southern is compared to summer northern).

3.6. Mixing Model

[31] The percent riverwater present at plume stations (%R = $r/(r + s)$) ranged between 3 and 22%. Stations with lower salinity and a higher proportional contribution of riverwater were not necessarily closer to the river mouth. Mixing model solutions for nonplume SML samples consistently returned small values for the riverwater proportion (r). The mean A_r endmember for plume samples was 253.3 ± 9.5 μeq kg^{-1} (n = 25), making the mean DIC_r = 308.8 ± 11.6 μmol kg^{-1} (n = 25, Table 2).

[32] Variations in DIC unexplained by the mixing model (ΔDIC_{BIO}) were up to 93 μmol C kg^{-1} at mid-range salinities (Figure 6). Plume summer stations generally had significantly positive ΔDIC_{BIO}, whereas only station 43 had a significantly negative ΔDIC_{BIO}. As well as having oversaturated pCO_2 and a homogenous water column, station 43 was located on the 80 m continental shelf and CDOM levels were especially high. Of the 17 plume stations with positive ΔDIC_{BIO}, the diazotrophic cyanobacteria *Trichodesmium* spp. was especially prevalent at 7 stations; diatoms (*Hemiaulus hauckii*) containing the diazotrophic endosymbiont *Richelia intracellularis* were especially abundant at 3 stations (sampled multiple times as part of a time series); and large quantities of both *Trichodesmium* and *Richelia* were found at 3 stations (Figure 6). Although there was no bottle-to-bottle correlation between ΔDIC_{BIO} and algal biomass at discrete depths, a significant positive correlation was found between ΔDIC_{BIO} in the plume and the integrated *Richelia* biomass at a given station (r = 0.707; n = 29, p < 0.001). The six samples with the greatest deviation from expected DIC values (ΔDIC_{BIO} = 60–95 μmol C kg^{-1}) were associated with large blooms of *Richelia*; other plume stations with either *Trichodesmium* or no prevailing diazotroph population showed smaller deviations between 10–40 μmol mol C kg^{-1}. If all production occurs in a 10 m-deep plume and ΔDIC_{BIO} represents a homogeneous DIC deficit at a plume station, then the depth-integrated biological DIC deficit in the plume (excluding station 43) would range between 0.1 and 0.9 mol C m^{-2}, with an average of 0.4 ± 0.06 mol C m^{-2} (n = 24).

[33] In nearly all cases, the pCO_2 expected from conservative mixing, pCO_{2exp}, was higher than the pCO_2 calculated from observed DIC and TA (pCO_{2obs}, equal to pCO_2(SST)) at plume stations (Figure 7). Conservative mixing is expected to drive pCO_2 below atmospheric pCO_2 consistently at salinities less than 33 (Figure 7). The pCO_{2obs} at plume stations was routinely about 30 μatm lower than pCO_{2exp}. At plume stations such as 23 and 27, where large numbers of *Hemiaulus/Richelia* were observed, in situ biological activity appears to intensify the sink by lowering pCO_2 60–120 μatm below expected levels.

4. Discussion

4.1. Nonplume WTNA

[34] In the absence of the Amazon River plume, modest seasonal changes in WTNA meteorology (Figure 4) drive changes in modeled mixed layer depths and mixed layer inventories (Table 4). Winter winds and net evaporation promote mixed-layer deepening and increases of salt and

Table 4. Mixed Layer Model Results for the WTNA Surface Mixed Layer (SML; ±1 SE) in Winter and Summer 2001

	Winter[a]	Summer, Southern	Summer, Northern
	Jan 19–Feb 22	Jul 14–Aug 15	
Stations	(n = 24)	(n = 4)	(n = 4)
Observed SML depth, m	78.5 ± 4.5	54.3 ± 8.1	76.0 ± 10.6
Model Output (+ freshwater effects on DIC)			
Duration, days	31	32	32
Mean SML depth, m	74.9 ± 0.2	15.0 ± 0.5	14.4 ± 0.4
SML Salinity change,[b] psu d^{-1}	+ 0.003	−0.0009	−0.0005
SML Salinity change, g salt m^{-3} d^{-1}	+ 3.3	−0.9	−0.5
SML Salinity inventory change,[c] mg m^{-2} s^{-1}	+ 2.8	−0.2	−0.1
SML DIC change, μmol kg^{-1} d^{-1}	+ 0.36	−0.034	−0.015
SML DIC inventory change, mmol C m^{-2} d^{-1}	+27	−0.53	−0.22
Model Output (− freshwater effects on DIC)[d]			
SML DIC change, μmol kg^{-1} d^{-1}	+0.21	+0.026	+0.041
SML DIC inventory change, mmol C m^{-2} d^{-1}	+16	+0.39	+0.61
Change in SML DIC inventory due to evaporation/precipitation,[e] mmol C m^{-2} d^{-1}	+11	−0.92	−0.83

[a]The winter run was forced with daily NCEP meteorological output, and the summer runs were forced with hourly average underway data (see Methods).
[b]Change in SML concentration $\Delta C = (C_{final} - C_{initial})$/Duration.
[c]Inventory change = ΔC*(Density)*(Mean SML depth). SML salt inventory change (storage) is presented per second to facilitate comparison with the literature (see Discussion).
[d]All other model outputs for II (e.g., MLD, salinity changes) were the same as the results listed for run I above.
[e]The difference between SML DIC inventory changes calculated during the two model runs.

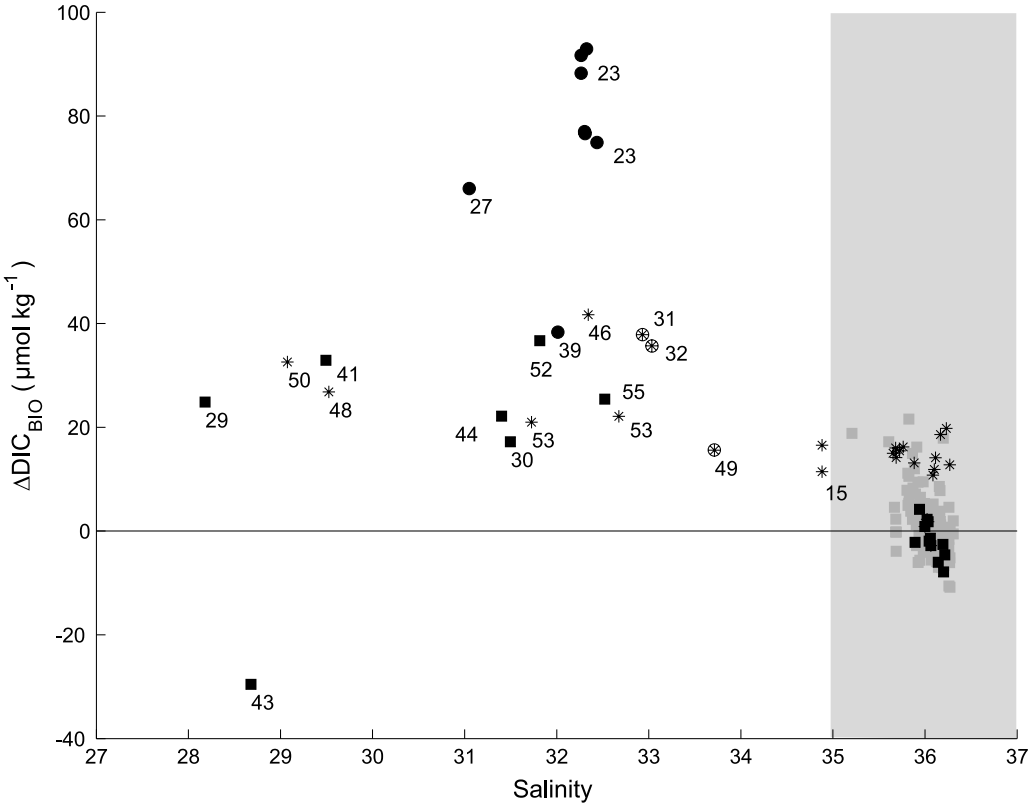

Figure 6. Community impact on DIC (ΔDIC_{BIO}), calculated with the mixing model, plotted against salinity. The 95% confidence interval error bars are within the size of the marker. Station numbers are shown for summer samples. Endmembers used to calculate ΔDIC_{BIO} included: $A_s = 2359.4 \pm 5.9$, $S_s = 36.07 \pm 0.10$, $DIC_s = 2024.5 \pm 6.8$, $S_r = 0 \pm 0$. The shaded region above salinity 35 indicates data outside the influence of the plume. Markers indicate the prevailing macroscopic nitrogen-fixing organisms observed at a station: square, none; circle, *Richelia*; asterisk, *Trichodesmium*; circle and star superimposed, *Richelia* and *Trichodesmium* together.

DIC. The late-summer drop in wind, followed by increased fall precipitation [see *Yoo and Carton*, 1990, Figure 3c], promotes mixed-layer shoaling and a small mixed-layer decrease in salinity and DIC. The large sensitivity of WTNA mixed layers to the freshwater balance differs from the familiar convectively driven North Atlantic model, in which winter cooling and high winds promote deep mixing until summer's warm temperatures and calmer conditions stratify the water column [e.g., *Hansell and Carlson*, 2001; *Michaels et al.*, 1994, and references therein].

[35] Although our PWP model results for SML DIC predict an increase in winter and a decrease in summer, observed mixed-layer WTNA DIC and TA concentrations outside the plume vary little between seasons (these data, GEOSECS, WOCE, and ETAMBOT/SABORD data). Invoking seasonally varying air-sea gas transfer to balance the carbon budget is insufficient to explain the observed lack of seasonal DIC change. At winter and summer southern nonplume stations, the favored direction of air-sea gas transfer enhances the SML carbon inventory change (Tables 3 and 4 and Figure 8). Only north of the plume in summer does air-sea exchange oppose the net change in SML carbon inventory (Table 4 and Figure 8). In short, the favored direction of air-sea carbon transfer often drives the system further from steady state.

[36] Estimating the vertical fluxes, by removing the effects of precipitation and evaporation on modeled SML DIC, highlights the strong influence of the freshwater balance on regional carbon inventories, but still does not help balance the budget. In summer, the vertical flux is very small, and precipitation-driven changes cause the observed loss in SML carbon. In contrast, the winter vertical flux is large and accounts for over half the SML carbon inventory increase (Figure 8). To maintain the small seasonal differences we observed in the WTNA nonplume, predicted carbon inventory changes must be offset by additional seasonally varying processes such as plume-ocean mixing, horizontal advection, or export.

[37] Summer northern WTNA nonplume stations are in position to receive retroflected plume water, which is characterized by low pCO_2 and salinity. Although the small difference between SML salinities north and south of the plume is not statistically significant (data not shown), the significant, temperature-independent difference between the groups' pCO_2(SST) (Table 3) suggests that northern stations contain a small amount of plume water. The pCO_2 undersaturation at these stations will be replaced slowly, because both the vertical carbon flux (+0.61 mmol C m^{-2} d^{-1}) and air-sea gas transfer (+1.6 mmol C m^{-2} d^{-1}) into the SML are quite small.

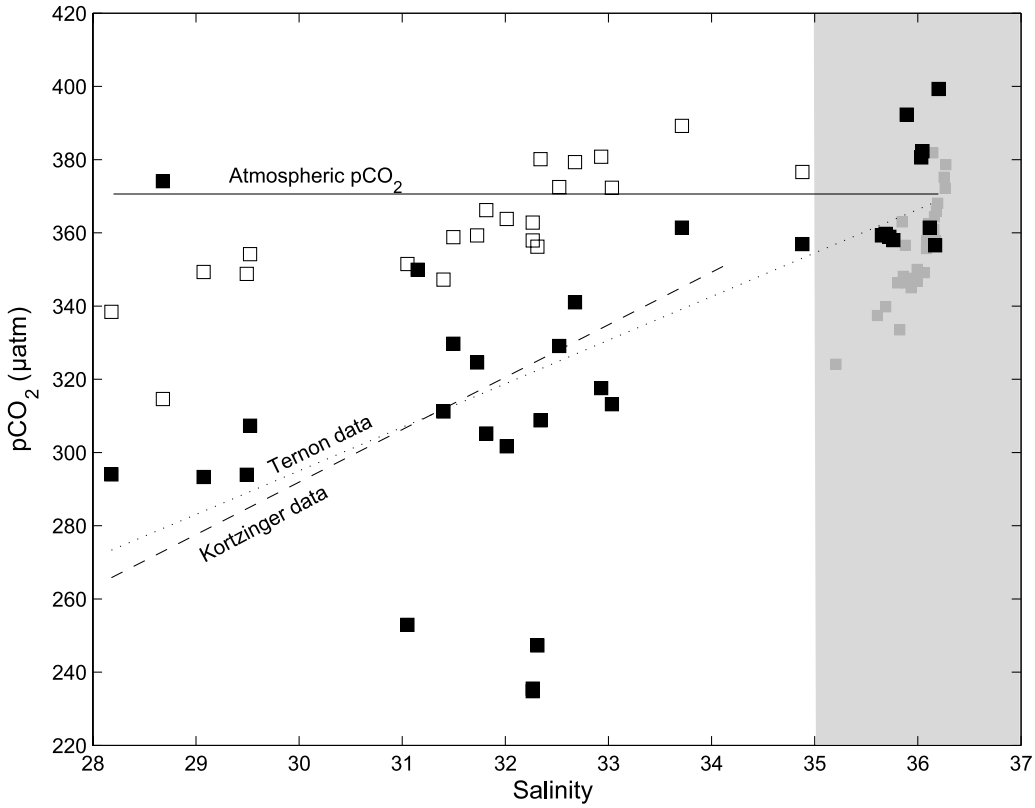

Figure 7. Winter (dark gray squares) and summer pCO_2 (black squares) calculated at SST are plotted against salinity. Open squares indicate expected pCO_2 (pCO_{2exp}), given conservative mixing of plume and ocean water. Regressions of ETAMBOT/SABORD data, and *Meteor* cruise 55 data are shown for comparison. The shaded region above salinity 35 indicates data outside the influence of the plume.

[38] A three-dimensional salinity budget at the nearby PIRATA array (4–15°N, 38°W) indicates that advection varies seasonally in the tropical Atlantic and can significantly affect the SML concentrations of dissolved constituents [*Foltz et al.*, 2004]. In February, advection at the 8°N, 38°W buoy contributes −1 mg m^{-2} s^{-1} salt to the total accumulation of +2 ± 1.5 mg m^{-2} s^{-1} [*Foltz et al.*, 2004]. If similar horizontal advection were applied to our mod-

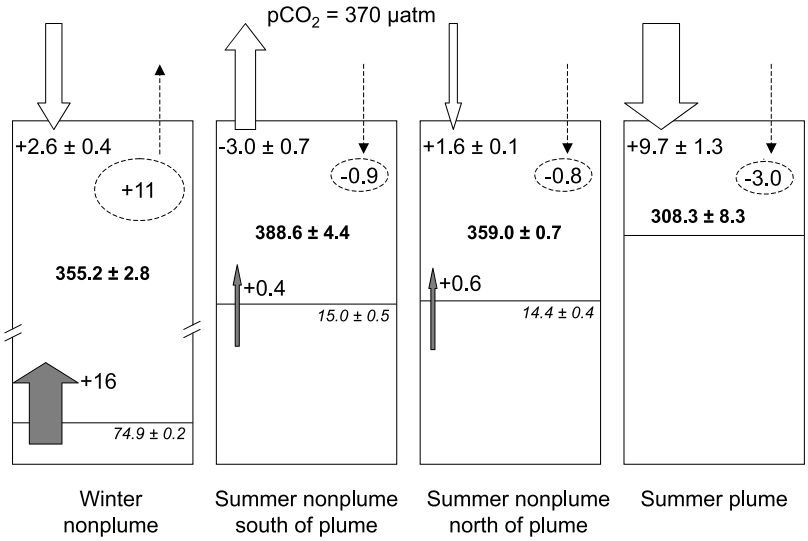

Figure 8. Schematic diagram of physical influences on the one-dimensional, WTNA surface mixed layer carbon budget. All fluxes are in mmol m^{-2} d^{-1}. Solid lines indicate mixed layer depth (m). White arrows represent air-sea CO_2 transfer, and gray arrows represent vertical mixing fluxes. Dashed arrows indicate net evaporation (up) or precipitation (down), and numbers in the dashed ovals indicate the associated change per day in the surface mixed layer carbon inventory (see Methods and Discussion).

eled salinity increase (+2.8 mg m^{-2} s^{-1}), the net WTNA salinity increase would be 1.8 mg m^{-2} s^{-1}, which agrees with the net increase of *Foltz et al.* [2004]. Later, advection and precipitation at the PIRATA mooring site increase, removing accumulated salt [*Foltz et al.*, 2004] and, presumably, DIC.

[39] While mixing, air-sea gas exchange, and advection physically alter SML DIC concentrations in the nonplume WTNA, low levels of biological activity may also remove some of the predicted winter and northern summer DIC accumulation, and intensify the predicted southern summer nonplume DIC loss. Observed primary production rates in the oligotrophic Atlantic Ocean are 2–30 mmol C m^{-2} d^{-1} [*Maranon et al.*, 2003], with higher rates in the WTNA during *Richelia/Hemiaulus* blooms (100 mmol C m^{-2} d^{-1} [*Carpenter et al.*, 1999], although these large blooms tend to occur in fresher waters) which could remove significant amounts of DIC. If 10% of primary production is exported [*Broecker*, 1974], 0.2–10 mmol C m^{-2} d^{-1} of the expected DIC accumulation (accounting for 15–>100% of the summer northern total and 0.1–38% of the winter total) can be removed biologically. In comparison, biological production in the winter 2001 Eastern Equatorial Pacific removed 17% of SML DIC in a system dominated by air-sea gas exchange and upwelling [*Sabine et al.*, 2004]. In the absence of the river plume, the WTNA inorganic carbon budget therefore appears to be most affected by physical influences on the water column, but uncertainties in removal terms underscore the importance of better understanding the timing and magnitude of both advection and export in the WTNA carbon cycle.

4.2. Plume-Influenced WTNA

[40] In the plume-influenced WTNA, low-salinity, low-carbon Amazon water remains atop the water column in a coherent lens and alters physical conditions in the SML. A strong pycnocline separating plume and ocean water hampers vertical mixing [*Pailler et al.*, 1999; *Sprintall and Tomczak*, 1992], forces a shallow mixed layer, and necessarily attenuates the upward carbon flux. Together, air-sea CO_2 transfer and net precipitation (Figure 8) only add 3.8% of the observed inorganic carbon increase between the river and the ocean. Without large carbon fluxes into the plume, DIC and TA distributions in the offshore plume therefore reflect primarily conservative mixing (presumably lateral) between river and ocean water (Figure 3 and Table 1) [*Ternon et al.*, 2000; *Körtzinger*, 2003]. Gas exchange, evaporation, and biology (see below) determine only the smaller residual differences between the conservative mixing line and the observations.

[41] Biological processes influence DIC throughout the plume [*Muller-Karger et al.*, 1988; *Longhurst*, 1993; *Muller-Karger et al.*, 1995; *Ternon et al.*, 2000; *Körtzinger*, 2003; *Benner et al.*, 1995; *Richey et al.*, 1990; *Demaster and Pope*, 1996; *Aller et al.*, 1996; *Devol et al.*, 1987]. Respiration in the early plume supported by river-borne organic matter releases CO_2 [*Benner et al.*, 1995; *Richey et al.*, 1990; *Demaster and Pope*, 1996; *Aller et al.*, 1996; *Devol et al.*, 1987], creating areas like station 43, whose high pCO_2 and CDOM suggested terrestrial DOM was being respired [*Smith and DeMaster*, 1996; *Del Vecchio and Subramaniam*, 2004; *Demaster and Pope*, 1996]. Further offshore, lower turbidity allows production to exceed respiration [*Demaster et al.*, 1996], permitting enhancement of the mixing-induced sink by causing additional decreases in pCO_2 (Station 23, Figures 5, 6, and 7 [*Ternon et al.*, 2000; *Körtzinger*, 2003]). Meanwhile, growth of carbonate-forming organisms could alter plume TA nonconservatively, but they were not observed on these cruises (E. J. Carpenter, personal communication) and are not common in the WTNA [*Kinkel et al.*, 2000; *Iglesias-Rodriguez et al.*, 2002].

4.3. Quantifying the Influence of Biology on Plume Waters

[42] During an algal bloom, production and export remove SML inorganic carbon faster than gas exchange and vertical mixing replace it, decreasing DIC in proportion to net community production. In this study, typical ΔDIC_{BIO} values were about 20 μmol kg^{-1}, with the highest values found at diazotroph-dominated stations (Figure 6). If these near-surface samples reflected conditions throughout the SML, depth-integrated inorganic carbon deficits were approximately 200 mmol C m^{-2}. Steadily exporting 10% of diazotroph-associated primary production (reported rates for *Trichodesmium* and *Richelia*-rich communities are 67–93 mmol C m^{-2} d^{-1} [*Carpenter et al.*, 2004, 1999]) would generate this integrated deficit in 22 to 30 days. Export may occur in even less time; salp swarms observed feeding on diazotroph-rich communities in summer (E. J. Carpenter, personal communication) could periodically increase export. Our results suggest that WTNA carbon sequestration depends on algal community structure.

[43] Using ΔDIC_{BIO} as a direct proxy for export neglects the likelihood that some dissolved and particulate organic material remains in the mixed layer (DOC, POC), and that physical processes such as air-sea exchange start reducing inorganic carbon deficits as soon as they are created. Lacking organic matter data for the 2001 cruises, we assume the WTNA POC pool behaves similarly to that of BATS, where the euphotic zone suspended particle stock is constant (25–35 μg kg^{-1}) between seasons [*Bates et al.*, 1996]. We also assume WTNA DOC production is similar to that of the oligotrophic open ocean, comprising 10–20% of net community production [*Hansell and Carlson*, 1998]. As a result, ΔDIC_{BIO}- based export estimates could overestimate the downward carbon flux by 10–20%. On the other hand, not including the effects of air-sea replacement and net precipitation in the mixing model may cause ΔDIC_{BIO} to underestimate net community production. Observed deficits (the net result of biological and physical processes) were 20–90 μmol C kg^{-1}, so our biological impact estimates could more than double if physical effects are included (adding up to 56 μmol C kg^{-1} over an 80-day transit). Patchy blooms [e.g., *Carpenter et al.*, 1999] remove plume DIC over days to weeks, whereas steady physical processes add DIC over weeks to months. In total, ΔDIC_{BIO}-based numbers likely underestimate biological impacts on the plume carbon cycle because ongoing physical processes likely add more carbon to the deficit than DOC production removes. More information on the timing of biological production and export in the WTNA is required to calculate biological impacts on WTNA DIC precisely. For example, deficits from early-plume bloom/export cycles could be completely replaced by physical processes before the water mass was

sampled, causing large underestimates of ΔDIC_{BIO}. Further along the mixing gradient, export could create large DIC deficits that were only partially replaced by physical processes at the time of sampling. In this case, our export estimates would be more accurate. Although the timescale of ΔDIC_{BIO} accumulation is not precisely known, we conclude that enough time elapses during the plume transit to accumulate measurable ΔDIC_{BIO} representative of integrated biological impacts on the plume.

[44] The consistent positive difference between pCO_{2exp} and $pCO2_{obs}$ at plume stations regardless of diazotroph abundance (about 30 μatm; Figure 7) supports the hypothesis that inorganic carbon deficits in the outer plume carry the integrated record of biological drawdown over some period of the plume's travel time. The conservative mixing model data, the observed temperature-independent pCO_2 undersaturation at northerly WTNA nonplume stations, and the mixed layer model results suggest that after the plume structure breaks down, a lasting small carbon deficit initiated by physical mixing and enhanced by biological drawdown is distributed over a deep SML. In that situation, both air-sea and vertical carbon fluxes are slow, lengthening the time to replace the carbon deficit. Thus, the Amazon plume causes a portion of the oceanic-salinity WTNA to take up atmospheric carbon, expanding the area and duration of the plume-related sink and opposing the expected paradigm of CO_2 release from tropical seawater.

[45] Our estimate of ΔDIC_{BIO} relies on some assumptions about river chemistry, because little is known about the carbonate system in the early plume. Previous studies used river DIC and TA measured at Obidos (1400 km upstream) to predict mixing curves for the carbonate system in the offshore plume [*Ternon et al.*, 2000]. However, several rivers from low-carbonate watersheds flow into the Amazon between Obidos and the estuary [*Devol and Hedges*, 2001], and carbonate system equilibria in river water shift upon meeting ocean water [*Körtzinger*, 2003; *Lewis and Wallace*, 1998]; therefore, early plume DIC and TA values are likely different from upstream river values. To date, only 1 DIC value (374 μM, November 1991 [*Druffel et al.*, 2005]) has been published for the zero salinity, early plume water (referred to as "river" water in our mixing model). A single hand sample collected for us in this zone during April 2002 had salinity of zero and TA of 440.71 ± 0.37 (±s.d., n = 2; S. R. Cooley, unpublished data). The *Druffel et al.* [2005] DIC value is closer to our solved DIC_r than the upriver value of DIC_r = 600 used previously [*Ternon et al.*, 2000, and references therein], suggesting that solving for A_r and DIC_r may introduce less error into this model of a poorly characterized system. The 0.82 TA:DIC ratio may indeed change in the near-shore mixing zone, but it is not likely to exceed unity until salinity increases above zero. If we instead used a ratio of 1 [see *Ternon et al.*, 2000], ΔDIC_{BIO} estimates would be about 40% smaller at the lowest-salinity stations (e.g., stations 29, 41, 48, 51), and 10–20% lower for samples with salinities 32–35.

5. Conclusions

[46] The seasonal appearance of the Amazon plume creates a high-nutrient, low-carbon incubator that is somewhat isolated from the oligotrophic water column beneath. DIC and TA distributions in our samples (27 < S < 36) reflect primarily conservative mixing between the ocean and the river, but biologically induced variations in DIC accumulate because of rapid production and slow carbon replacement. Most of the WTNA stations with DIC deficits occurred where high numbers of *Trichodesmium* or *Richelia*/diatom symbioses were found, suggesting that diazotrophic activity is associated with increased carbon drawdown in the Amazon plume. Stations with high *Richelia*/diatom concentrations tended to have greater deficits than other stations. These deficits enhance and prolong the undersaturation of the plume. In the absence of the Amazon River plume, inorganic carbon cycling in the WTNA was dominated by physical processes such as the freshwater balance, air-sea gas exchange, and vertical entrainment, but accounting for two- or three-dimensional processes is required to explain the observed lack of seasonality in the nonplume DIC inventory. Our calculations show that residual DIC deficits both from river dilution and biological activity may endure for many months, and reduce the overall tendency of the WTNA to outgas CO_2.

[47] **Acknowledgments.** This research was supported by the Office of Science (BER), U.S. Department of Energy, grant DE-FG02-02ER63472, NOAA Office of Global Programs grant NA16GP2689, and by faculty research support from the University of Georgia to P.L.Y. Financial support was provided to S.R.C. by the University of Georgia Presidential Graduate Fellowship and the NASA Earth System Science Fellowship. A. F. Michaels, D. G. Capone, and E. J. Carpenter graciously invited us into the MANTRA/PIRANA Biocomplexity Project. E. J. Carpenter, D. G. Capone, A. Subramaniam, and M. Neumann shared data with us and provided excellent sampling access. M. J. Erickson assisted with sampling and offered helpful insight. A. Goodrich assisted with sample analysis. A. B. Burd and V. Coles provided technical assistance and guidance on the Monte Carlo-type model. F. le Hingrat at IFREMER made the ETAMBOT/SABORD data sets available. A. Kortzinger made the Meteor 55 pCO_2 data set available. D. Di Iorio and J. Christian provided helpful commentary regarding the PWP model. The manuscript was greatly improved by the comments of B. Hales, one anonymous reviewer, A. Burd, V. Coles, and J. C. Fisher.

References

Aller, R. C., N. E. Blair, Q. Xia, and P. D. Rude (1996), Remineralization rates, recycling, and storage of carbon in Amazon shelf sediments, *Cont. Shelf Res.*, *16*, 753–786.

Bates, N. R., A. F. Michaels, and A. H. Knap (1996), Seasonal and interannual variability of oceanic carbon dioxide species at the US JGOFS Bermuda Atlantic Time-series Study (BATS) site, *Deep Sea Res., Part II.*, *43*(2–3), 347–383.

Bauer, J., C. Reimers, E. Druffel, and P. Williams (1995), Isotopic constraints on carbon exchanges between deep ocean sediments and seawater, *Nature*, *373*, 686–689.

Bender, M., et al. (1987), A comparison of four methods for determining planktonic community production, *Limnol. Oceanogr.*, *32*(5), 1085–1098.

Benner, R., S. Opsahl, G. Chin-Leo, J. E. Richey, and B. R. Forsberg (1995), Bacterial carbon metabolism in the Amazon River system, *Limnol. Oceanogr.*, *40*(7), 1262–1270.

Bourles, B., Y. Gouriou, and R. Chuchla (1999), On the circulation in the upper layer of the western equatorial Atlantic, *J. Geophys. Res.*, *104*(C9), 21,151–21,170.

Brainerd, K. E., and M. C. Gregg (1995), Surface mixed and mixing layer depths, *Deep Sea Res., Part I*, *42*(9), 1521–1543.

Broecker, W. S. (1974), *Chemical Oceanography*, Harcourt Brace Jovanovich, New York.

Capone, D. G., J. P. Zehr, H. W. Paerl, B. Bergman, and E. J. Carpenter (1997), *Trichodesmium*, a globally significant marine cyanobacterium, *Science*, *276*, 1221–1229.

Carpenter, E. J., J. P. Montoya, J. Burns, M. R. Mulholland, and A. Subramaniam (1999), Extensive bloom of a N_2-fixing diatom/cyanobacterial association in the tropical Atlantic Ocean, *Mar. Ecol. Prog. Ser.*, *185*, 273–283.

Carpenter, E. J., A. Subramaniam, and D. G. Capone (2004), Biomass and primary productivity of the cyanobacterium *Trichodesmium* spp. in the tropical N. Atlantic Ocean, *Deep Sea Res.*, *51*, 173–203.

del Giorgio, P. A., J. J. Cole, and A. Cimbleris (1997), Respiration rates in bacteria exceed phytoplankton production in unproductive aquatic systems, *Nature*, *385*, 148–151.

Del Vecchio, R., and A. Subramaniam (2004), Influence of the Amazon River on the surface optical properties of the Western Tropical North Atlantic Ocean, *J. Geophys. Res.*, *109*, C11001, doi:10.1029/2004JC002503.

Demaster, D. J., and R. C. Aller (2001), Biogeochemical processes on the Amazon Shelf: Changes in dissolved and particulate fluxes during river/ocean mixing, in *The Biogeochemistry of the Amazon Basin*, edited by M. E. McClain, R. L. Victoria, and J. E. Richey, pp. 328–357, Oxford Univ. Press, New York.

Demaster, D. J., and R. H. Pope (1996), Nutrient dynamics in Amazon shelf waters - Results from Amasseds, *Cont. Shelf Res.*, *16*(3), 263–289.

Demaster, D. J., W. O. Smith, D. M. Nelson, and J. Y. Aller (1996), Biogeochemical processes in Amazon shelf waters: Chemical distributions and uptake rates of silicon, carbon and nitrogen, *Cont. Shelf Res.*, *16*(5–6), 617–643.

Devol, A. H., and J. I. Hedges (2001), Organic matter and nutrients in the mainstem Amazon River, in *The Biogeochemistry of the Amazon Basin*, edited by M. E. McClain, R. L. Victoria, and J. E. Richey, pp. 275–306, Oxford Univ. Press, New York.

Devol, A. H., P. D. Quay, J. E. Richey, and L. A. Martinelli (1987), The role of gas exchange in the inorganic carbon, oxygen, and 222-Rn budgets of the Amazon River, *Limnol. Oceanogr.*, *32*(1), 235–248.

Dickson, A. G. (1990), Standard potential of the reaction: $AgCl_{(s)} + 1/2\ H_{2(g)} = Ag_{(s)} + HCl_{(aq)}$, and the standard acidity constant of the ion $HSO_4^{(-)}$ in synthetic seawater from 273.15 to 318.15K, *J. Chem. Thermodyn.*, *22*, 113–127.

Dickson, A. G., and F. J. Millero (1987), A comparison of the equilibrium constants for the dissociation of carbonic acid in seawater media, *Deep Sea Res., Part A*, *34*(10), 1733–1743.

Dickson, A. G., J. D. Afghan, and G. C. Anderson (2003), Reference materials for oceanic CO_2 analysis: a method for the certification of total alkalinity, *Mar. Chem.*, *80*, 185–197.

DOE (1997), Handbook of methods for the analysis of the various parameters of the carbon dioxide system in sea water, edited by A. G. Dickson and C. Goyet, *ORNL/CDIAC-74*, Oak Ridge Natl. Lab., Oak Ridge, Tenn.

Druffel, E., J. Bauer, and S. Griffin (2005), Input of particulate organic and dissolved inorganic carbon from the Amazon to the Atlantic Ocean, *Geochem. Geophys. Geosyst.*, *6*, Q03009, doi:10.1029/2004GC000842.

Duarte, C. M., and S. Agustí (1998), The CO_2 balance of unproductive aquatic ecosystems, *Science*, *281*, 234–236.

Duarte, C. M., S. Agusti, J. Aristegui, N. González, and R. Anadón (2001), Evidence for a heterotrophic subtropical northeast Atlantic, *Limnol. Oceanogr.*, *46*(2), 425–428.

Edmond, J. M., E. A. Boyle, B. Grant, and R. F. Stallard (1981), The chemical mass balance in the Amazon plume - I. The nutrients, *Deep Sea Res.*, *28*, 1339–1374.

Ferry, N., and G. Reverdin (2004), Sea surface salinity interannual variability in the western tropical Atlantic: An ocean general circulation model study, *J. Geophys. Res.*, *109*, C05026, doi:10.1029/2003JC002122.

Foltz, G. R., S. A. Grodsky, J. A. Carton, and M. J. McPhaden (2004), Seasonal salt budget of the northwestern tropical Atlantic Ocean along 38°W, *J. Geophys. Res.*, *109*, C03052, doi:10.1029/2003JC002111.

Geider, R. J. (1997), Photosynthesis or planktonic respiration?, *Nature*, *388*, 132–133.

Geyer, W. R. (1991), The physical oceanography of Amazon outflow, *Oceanography*, *4*, 8–14.

Geyer, W. R., R. C. Beardsley, S. J. Lentz, J. Candela, R. Limeburner, W. E. Johns, B. M. Castro, and I. D. Soares (1996), Physical oceanography of the Amazon shelf, *Cont. Shelf Res.*, *16*(5–6), 575–616.

Gill, A. E. (1982), *Atmosphere-Ocean Dynamics*, Elsevier, New York.

Goyet, C., R. Adams, and G. Eischeid (1998), Observations of the CO_2 system properties in the tropical Atlantic Ocean, *Mar. Chem.*, *60*(1–2), 49–61.

Hansell, D. A., and C. A. Carlson (1998), Net community production of dissolved organic carbon, *Global Biogeochem. Cycles*, *12*(3), 443–453.

Hansell, D. A., and C. A. Carlson (2001), Biogeochemistry of total organic carbon and nitrogen in the Sargasso Sea: control by convective overturn, *Deep Sea Res., Part II*, *48*, 1649–1667.

Hellweger, F. L., and A. L. Gordon (2002), Tracing Amazon River water into the Caribbean Sea, *J. Mar. Res.*, *60*(4), 537–549.

Iglesias-Rodriguez, M. D., C. W. Brown, S. C. Doney, J. A. Kleypas, D. Kolber, Z. S. Kolber, P. K. Hayes, and P. G. Falkowski (2002), Representing key phytoplankton functional groups in ocean carbon cycle models: Coccolithophorids, *Global Biogeochem. Cycles*, *16*(4), 1100, doi:10.1029/2001GB001454.

Johns, W. E., T. N. Lee, R. C. Beardsley, J. Candela, R. Limeburner, and B. Castro (1998), Annual cycle and variability of the North Brazil Current, *J. Phys. Oceanogr.*, *28*(1), 103–128.

Johnson, K. M., K. D. Wills, D. B. Butler, W. K. Johnson, and W. S. Wong (1993), Coulometric total carbon-dioxide analysis for marine studies: Maximizing the performance of an automated gas extraction system and coulometric detector, *Mar. Chem.*, *44*, 167–187.

Kalnay, E., et al. (1996), The NCEP/NCAR 40-Year Reanalysis Project, *Bull. Am. Meteorol. Soc.*, *77*(3), 437–471.

Kinkel, H., K.-H. Baumann, and M. Cepek (2000), Coccolithophores in the equatorial Atlantic Ocean: response to seasonal and Late Quaternary surface water variability, *Mar. Micropaleontol.*, *39*, 87–112.

Körtzinger, A. (2003), A significant CO_2 sink in the tropical Atlantic Ocean associated with the Amazon River plume, *Geophys. Res. Lett.*, *30*(24), 2287, doi:10.1029/2003GL018841.

Ledwell, J. R., A. J. Watson, and C. S. Law (1993), Evidence for slow mixing across the pycnocline from an open-ocean tracer-release experiment, *Nature*, *364*, 701–703.

Lee, K., F. J. Millero, and R. Wanninkhof (1997), The carbon dioxide system in the Atlantic Ocean, *J. Geophys. Res.*, *102*(C7), 15,693–15,707.

Lentz, S. J. (1995), Seasonal variations in the horizontal structure of the Amazon plume inferred from historical hydrographic data, *J. Geophys. Res.*, *100*(C2), 2391–2400.

Lentz, S. J., and R. Limeburner (1995), The Amazon River plume during AMASSEDS: Spatial characteristics and salinity variability, *J. Geophys. Res.*, *100*(C2), 2355–2375.

Lewis, E., and D. W. R. Wallace (1998), Program developed for CO_2 system calculations, version 1.05, *ORNL/CDIAC-105*, Carbon Dioxide Inf. Anal. Cent., Oak Ridge Natl. Lab., U.S. Dep. of Energy, Oak Ridge, Tenn.

Longhurst, A. (1993), Seasonal cooling and blooming in tropical oceans, *Deep Sea Res., Part I*, *40*, 2145–2165.

Mackenzie, F. T., A. Lerman, and L. M. B. Ver (1998), Role of the continental margin in the global carbon balance during the past three centuries, *Geology*, *26*(5), 423–426.

Maranon, E., M. J. Behrenfeld, N. González, B. Mouriño, and M. V. Zubkov (2003), High variability of primary production in oligotrophic waters of the Atlantic Ocean: uncoupling from phytoplankton biomass and size structure, *Mar. Ecol. Prog. Ser.*, *257*, 1–11.

Mehrbach, C., C. H. Culberson, J. E. Hawley, and R. M. Pytkowicz (1973), Measurement of apparent dissociation constants of carbonic acid in seawater at atmospheric pressure, *Limnol. Oceanogr.*, *18*(6), 897–907.

Michaels, A. F., et al. (1994), Seasonal patterns of ocean biogeochemistry at the US JGOFS Bermuda Atlantic Time-series Study site, *Deep Sea Res., Part I*, *41*, 1013–1038.

Millero, F. J., and A. Poisson (1981), International one-atmosphere equation of state for sea water, *Deep Sea Res.*, *28*, 625–629.

Millero, F. J., J.-Z. Zhang, K. Lee, and D. M. Campbell (1993), Titration alkalinity of seawater, *Mar. Chem.*, *44*, 153–165.

Muller-Karger, F. E., C. R. McClain, and P. L. Richardson (1988), The dispersal of the Amazon's water, *Nature*, *333*(56–59).

Muller-Karger, F. E., P. L. Richardson, and D. J. McGillicuddy (1995), On the offshore dispersal of the Amazon's plume in the North Atlantic: Comments, *Deep Sea Res., Part I*, *42*(11–12), 2127–2131.

Nittrouer, C. A., and D. J. Demaster (1986), Sedimentary processes on the Amazon continental shelf - Past, present and future research, *Cont. Shelf Res.*, *6*(1–2), 5–30.

Pailler, K., B. Bourles, and Y. Gouriou (1999), The barrier layer in the Western Tropical Atlantic Ocean, *Geophys. Res. Lett.*, *26*(14), 2069–2072.

Price, J. F., R. A. Weller, and R. Pinkel (1986), Diurnal cycling: Observations and models of the upper ocean response to diurnal heating, cooling, and wind mixing, *J. Geophys. Res.*, *91*, 8411–8427.

Richey, J. E., J. I. Hedges, A. H. Devol, P. D. Quay, R. L. Victoria, L. A. Martinelli, and B. R. Forsberg (1990), Biogeochemistry of carbon in the Amazon River, *Limnol. Oceanogr.*, *35*(2), 352–371.

Richey, J. E., R. L. Victoria, E. Salati, and B. R. Forsberg (1991), The biogeochemistry of a major river system: The Amazon case study, in *Biogeochemistry of Major World Rivers*, vol. 42, edited by E. T. Degens, S. Kempe, and J. E. Richey, pp. 57–74, John Wiley, Hoboken, N. J.

Sabine, C. L., R. A. Feely, G. C. Johnson, P. G. Strutton, M. F. Lamb, and K. E. McTaggart (2004), A mixed layer carbon budget for the GasEx-2001 experiment, *J. Geophys. Res.*, *109*, C08S05, doi:10.1029/2002JC001747.

Sarmiento, J. L., R. Murnane, and C. Lequere (1995), Air-sea CO_2 transfer and the carbon budget of the North Atlantic, *Philos. Trans. R. Soc. London, Ser. B*, *348*(1324), 211–219.

Serret, P., C. Robinson, E. Fernandez, E. Teira, and G. Tilstone (2001), Latitudinal variation of the balance between plankton photosynthesis and respiration in the eastern Atlantic Ocean, *Limnol. Oceanogr.*, *46*(7), 1642–1652.

Smith, W. O., Jr., and D. J. DeMaster (1996), Phytoplankton biomass and productivity in the Amazon River plume: correlation with seasonal river discharge, *Cont. Shelf Res.*, *16*(3), 291–319.

Sokal, R. R., and F. J. Rohlf (2000), *Biometry: The Principles and Practice of Statistics in Biological Research*, W. H. Freeman, New York.

Sprintall, J., and M. Tomczak (1992), Evidence of the barrier layer in the surface layer of the tropics, *J. Geophys. Res.*, *97*(C5), 7305–7316.

Sweeney, C., D. A. Hansell, C. A. Carlson, L. Codispoti, L. I. Gordon, J. Marra, F. J. Millero, W. O. Smith, and T. Takahashi (2000), Biogeochemical regimes, net community production and carbon export in the Ross Sea, Antarctica, *Deep Sea Res., Part II*, *47*(15–16), 3369–3394.

Takahashi, T., J. Olafsson, J. G. Goddard, D. Chipman, and S. C. Sutherland (1993), Seasonal variation of CO_2 and nutrients in the high-latitude surface oceans: A comparative study, *Global Biogeochem. Cycles*, *7*(4), 843–878.

Takahashi, T., R. A. Feely, R. F. Weiss, R. H. Wanninkhof, D. W. Chipman, S. C. Sutherland, and T. T. Takahashi (1997), Global air-sea flux of CO_2: An estimate based on measurements of sea-air pCO_2 difference, *Proc. Natl. Acad. Sci. U. S. A.*, *94*(16), 8292–8299.

Takahashi, T., et al. (2002), Global sea-air CO_2 flux based on climatological surface ocean pCO_2, and seasonal biological and temperature effects, *Deep Sea Res., Part II*, *49*, 1601–1622.

Ternon, J. F., C. Oudot, A. Dessier, and D. Diverres (2000), A seasonal tropical sink for atmospheric CO_2 in the Atlantic Ocean: the role of the Amazon River discharge, *Mar. Chem.*, *68*, 183–201.

Wanninkhof, R. (1992), Relationship between wind-speed and gas-exchange over the ocean, *J. Geophys. Res.*, *97*(C5), 7373–7382.

Wanninkhof, R., and W. R. McGillis (1999), A cubic relationship between airs-sea CO_2 exchange and wind speed, *Geophys. Res. Lett.*, *26*(13), 1889–1892.

Weiss, R. F. (1974), Carbon dioxide in water and seawater: The solubility of a nonideal gas, *Mar. Chem.*, *2*, 203–215.

Williams, P. J. L., and D. G. Bowers (1999), Regional carbon imbalances in the oceans, *Science*, *284*, 1735.

Williams, P. J. L. (1998), The balance of plankton respiration and photosynthesis in the open oceans, *Nature*, *394*, 55–57.

Yager, P. L., D. W. R. Wallace, K. M. Johnson, W. O. J. Smith, P. J. Minnett, and J. W. Deming (1995), The Northeast Water Polynya as an atmospheric CO_2 sink: A seasonal rectification hypothesis, *J. Geophys. Res.*, *100*(C3), 4389–4398.

Yelland, M., and P. K. Taylor (1996), Wind stress measurements from the open ocean, *J. Phys. Oceanogr.*, *26*(4), 541–558.

Yoo, J.-M., and J. A. Carton (1990), Annual and interannual variation of the freshwater budget in the Tropical Atlantic Ocean and the Caribbean Sea, *J. Phys. Oceanogr.*, *20*, 831–845.

S. R. Cooley and P. L. Yager, School of Marine Programs, University of Georgia, Athens, GA 30602-3636, USA. (pyager@uga.edu)